Time domain simulation of vortex-induced vibrations in stationary and oscillating flows

M.J. Thorsen[a,*], S. Sævik[a], C.M. Larsen[a]

[a]*Department of Marine Technology, Norwegian University of Science and Technology, 7491 Trondheim, Norway*

Abstract

This paper focuses on the further development of a previously published semi-empirical method for time domain simulation of vortex-induced vibrations (VIV). A new hydrodynamic damping formulation is given, and the necessary coefficients are found from experimental data. It is shown that the new model predicts the observed hydrodynamic damping in still water and for cross-flow oscillations in stationary incoming flow with high accuracy. Next, the excitation force model is optimized by simulating the VIV response of an elastic cylinder in a series of experiments with stationary flow. The optimization is performed by repeating the simulations until the best possible agreement with the experiments is found. The optimized model is then applied to simulate the cross-flow VIV of an elastic cylinder in oscillating flow, without introducing any changes to the hydrodynamic force modeling. By comparison with experiment, it is shown that the model predicts the frequency content, mode and amplitude of vibration with a high level of realism, and the amplitude modulations occurring at high Keulegan-Carpenter numbers are well captured. The model is also utilized to investigate the effect of increasing the maximum reduced velocity and the mass ratio of the elastic cylinder in oscillating flow. Simulations show that complex response patterns with multiple modes and frequencies appear when the maximum reduced velocity is increased. If, however, the mass ratio is increased by a factor of 5, a single mode dominates. This illustrates that, in oscillating flows, the mass ratio is important in determining the mode participation at high maximum reduced velocities.

Keywords: Vortex-induced vibrations, Elastic cylinders, Oscillating flow, Time domain, Simulation

1. Introduction

Slender structures such as pipelines and risers experience vortex-induced vibrations (VIV) when exposed to external fluid flow (Blevins, 1990). The vibrations are a result of the fluctuating lift and drag forces associated with flow separation and vortex shedding. Depending on the incoming flow and structural properties, significant dynamic stress may occur, causing fatigue damage accumulation which over time may lead to structural failure. Understanding and being able to predict VIV in realistic environmental conditions is therefore important to ensure the safety of slender structures.

A considerable amount of work has been done to increase the understanding of VIV, as reflected in the reviews by Sarpkaya (2004), Williamson and Govardhan (2004), Bearman (2011) and Wu et al. (2012). As the equations of motion governing viscous flow are difficult to solve, experiments have been the most important source of new insight. Examples of typical experiments are free vibration of elastically mounted rigid cylinders (Feng, 1968; Vikestad, 1998; Govardhan and Williamson, 2000; Jauvtis and Williamson, 2004) and cylinders undergoing forced motions (Sarpkaya, 1978; Moe and Wu, 1990; Morse and Williamson, 2009; Aglen and Larsen, 2011; Yin and Larsen, 2012). Experiments with long flexible structures have also been performed, both under controlled laboratory conditions (Chaplin et al., 2005; Trim et al., 2005; Huera-Huarte et al., 2014) and in more realistic field environments (Huse et al., 1998; Vandiver et al., 2006). These

*Corresponding author. Tel.: +47 735 50881
Email address: mats.j.thorsen@ntnu.no (M.J. Thorsen)

experiments focused on various flow situations such as uniform, sheared and stepped current, and in all cases the incoming flow was essentially stationary, i.e. constant in time.

In some situations, the relative current velocity may be non-stationary, either due to movement of the structure or oscillations in the incoming flow itself. For example, a riser connected to a floating platform will oscillate as a result of the wave-induced motions of the floater. The relative flow velocity caused by the riser moving back and forth in the water may cause vortex shedding and VIV if the motion amplitude is sufficiently large. VIV of an elastic cylinder in oscillating flow was studied experimentally by Fu et al. (2014). They found that the structure vibrated significantly due to vortex shedding, and noted some important differences compared to stationary flow VIV. For instance, they observed a characteristic developing process with vibrations continuously building up and dying out. VIV of spring mounted rigid cylinders in oscillating flow has previously been studied by several researchers such as Sarpkaya (1979) and Sumer and Fredsøe (1988).

In light of these experimental studies, and the fact that oscillating flows are relevant in several practical applications, the need for a mathematical model able to predict VIV in oscillating flows becomes evident. One possibility is to solve the Navier-Stokes equations numerically, but the required computational effort is generally large. The semi-empirical frequency domain methods VIVA (Triantafyllou et al., 1999), SHEAR7 (Vandiver and Li, 2005) and VIVANA (Larsen et al., 2009) are more efficient, but can only predict VIV in stationary flows. As illustrated by Chang et al. (2003), the wake-oscillator can be used to simulate VIV in time domain for unsteady flow situations, but no comparison with experiment was included in this study. Liao (2001) was able to predict VIV in unsteady flow based on a relationship between an equivalent reduced damping and the resulting vibration amplitude. Recently, Resvanis (2014) proposed a dimensionless parameter which can be used to determine if the response in unsteady flow will be similar to the response in steady flow.

An alternative method for simulating VIV in time domain was proposed by Thorsen et al. (2014a). In this semi-empirical method, the fluid forces are calculated based on the incoming flow velocity and the motion of the cross-section. The special feature is how synchronization between the vortex shedding and cylinder motion is taken into account. It has been shown that the model provides realistic results for several different cases, including flexible cylinders in uniform, sheared and stepped current (Thorsen et al., 2014b, 2015). The formulation includes no restriction on the time variability of the incoming flow velocity, which means it is theoretically suited for simulating VIV in oscillating flows. With this in mind, the outline of the present paper is as follows: Firstly, the original model (Thorsen et al., 2014a) is slightly modified to improve the prediction accuracy in stationary flows. Secondly, the improved model is used to simulate a flexible cylinder in oscillating flow. The experiment by Fu et al. (2014) is used for comparison, allowing for direct assessment of the prediction accuracy. Finally, the model is used to explore the effect of changing certain key parameters. For instance, the reduced velocity is increased beyond what was considered in the actual experiment, resulting in the appearance of complex vibration patterns.

2. Time domain VIV model

2.1. Hydrodynamic force model

A stationary cylinder in an incoming undisturbed flow is subjected to time varying forces. The force component parallel to the flow is called drag, while the perpendicular component is named lift. Due to the vortex shedding process, the lift force oscillates with a frequency $f_s = \mathrm{St}U/D$ called the Strouhal frequency, where D is the cylinder diameter and U is the velocity of the flow. The Strouhal number St is generally a function of the Reynolds number and the surface roughness of the cylinder, but in the subcritical Reynolds number range, St is nearly constant and close to 0.2 (Norberg, 2003). If the cylinder is flexible, it will vibrate as a result of the oscillating fluid forces, and the movement of the cylinder alters the surrounding flow and the corresponding fluid forces. One of the most important effects is that the vortex shedding may synchronize with the cylinder motion, such that the frequency of the lift force deviates from the expected Strouhal frequency. In addition, there will be fluid resistance (damping) and added mass effects due to the velocity and acceleration of the cylinder.

The hydrodynamic force model used here was first presented by Thorsen et al. (2014a). Some minor modifications were introduced (Thorsen et al., 2015), providing the starting point for the present paper. In these previous studies, hydrodynamic damping was modeled using a linear and quadratic term, and the empirical coefficients were found by minimizing the difference between this model and the model given by Venugopal (1996). Although this was quite successful, a tendency to over-predict the cross-flow vibration amplitude in uniform flow and under-predict it in linearly sheared flow was seen (Thorsen et al., 2015), which indicates that the model can still be improved. With this in mind, a new damping model is developed here, using actual measurements to adjust the empirical coefficients. As the total energy transfer between fluid and structure is determined from the energy delivered by the vortex shedding process and the energy subtracted by the hydrodynamic damping, altering the damping model will require a change in the excitation model to ensure that the net power transfer is physically correct. This is addressed further in section 3.

It should be pointed out that the new developments described in this section are based on data from experiments performed in stationary incoming flow. Hence, the model is directly tuned to accurately predict vortex-induced vibrations in stationary flows. As there are no mathematical restrictions on the time-variability of the incoming flow, it is straightforward to apply the model in oscillating flows as well. However, an oscillating flow will introduce some physical changes which are not taken into account in the model. Most importantly, the flow meeting the cylinder is no longer undisturbed, but contains previously shed vortices. In this context, an interesting question is: Can VIV in oscillating flows be predicted based on data from stationary flow VIV? An attempt to answer this question is made in section 4.

2.1.1. Cross-flow hydrodynamic force

Hydrodynamic damping (or drag) on circular cylinders has been extensively studied, see e.g. Sarpkaya (2010). For the present application, trying to develop a model which reproduces the true damping exactly in every situation would be disadvantageous, because such a model would be very complicated, and perhaps unrealizable without resorting to direct numerical simulation of the Navier-Stokes equations. A pragmatic point of view is therefore adopted, trying to find a damping model which is sufficiently accurate to represent the energy extraction in vortex-induced vibrations, while being applicable in a computationally efficient time domain simulation.

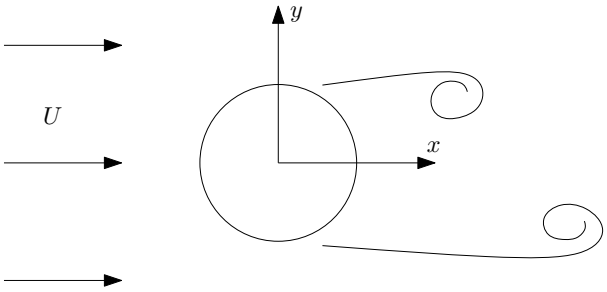

Figure 1: Cylinder with incoming flow and coordinate system definition.

Consider a cylinder cross-section with diameter D in an incoming undisturbed flow of velocity U and density ρ. Let the x-axis point in the direction of the flow, and the y-axis in the direction normal to the flow, as seen in figure 1. The origin is positioned at the center of the cylinder, such that y corresponds to the cross-flow displacement away from the position of static equilibrium. In the previous papers on this model, hydrodynamic damping was modeled using a linear and quadratic term. However, the accuracy is found to increase if the linear term is dropped, and the cross-flow hydrodynamic damping is now expressed as

$$F_{d,y} = -\frac{1}{2}\rho D C_{d,y}|\dot{y}|\dot{y}, \tag{1}$$

where $\dot{y}$ is the cross-flow velocity of the cylinder. A crucial step is to find an appropriate $C_{d,y}$. If $U = 0$, we have an oscillating cylinder in still water, which with respect to the drag force is equivalent to a fixed

cylinder in an oscillating flow. This case has been studied by Sarpkaya (1986), and it is found that $C_{d,y}$ depends strongly on the Keulegan-Carpenter number (KC), or equivalently, the ratio between the oscillation amplitude and the cylinder diameter. For simplicity, it is assumed that the damping coefficient can be expressed as a linear function of y_0/D over the relevant range, i.e. $C_{d,y} = a_0 + a_1 y_0/D$, where y_0 is the cross-flow amplitude of vibration. To find the appropriate values of a_0 and a_1, damping coefficients from still-water decay tests are utilized (Vikestad et al., 2000).

It is essential that the energy loss caused by the drag force given in equation (1) is the same as measured in experiments. If the energy loss is equal, so is the average power extracted by the damping force over one oscillation period. This can be expressed as:

$$\overline{\dot{W}}_{d,y} = \frac{1}{T}\int_0^T F_{d,y}\ \dot{y}\ dt, \tag{2}$$

where $T = 2\pi/\omega$ is the period. Inserting the damping force from equation (1) using $C_{d,y} = a_0 + a_1 y_0/D$ and $\dot{y} = \omega y_0 \cos\omega t$, the following result is obtained:

$$\overline{\dot{W}}_{d,y} = -\frac{1}{2T}\rho D(a_0 + a_1\frac{y_0}{D})\int_0^T |\dot{y}|\dot{y}^2 dt = -\frac{8}{12\pi}\rho D(a_0 + a_1\frac{y_0}{D})\omega^3 y_0^3. \tag{3}$$

Vikestad et al. (2000) expresses damping as a linear function of velocity, $F_{d,y} = -c\dot{y}$, and reports the damping coefficient c as a function of oscillation amplitude. Inserting the linear damping formulation in equation (2) gives

$$\overline{\dot{W}}_{d,y} = -\frac{1}{T}\int_0^T c\dot{y}^2 dt = -\frac{1}{2}c\omega^2 y_0^2. \tag{4}$$

Ideally, the right hand side of equations (3) and (4) should be equal for all oscillation amplitudes when c is the amplitude dependent damping measured in experiments. The method of least squares is used to find the values of a_0 and a_1 that minimize the sum of the square differences, resulting in $a_0 = 0.31$ and $a_1 = 0.89$. The power loss based on Vikestad's measurements and the present model is shown in figure 2. The results from the old damping model (Thorsen et al., 2014a) is also shown, and it is seen that the new model provides much better agreement with the experiment.

To investigate the performance when $U \neq 0$, the model is used to simulate the hydrodynamic damping force on a cylinder oscillating in the cross-flow direction with frequency f at a reduced velocity, $U_r = U/(fD)$ of 3 and 10, which is below and above the positive excitation zone respectively. The resulting lift coefficient in phase with cylinder velocity is compared to forced vibration experiments by Morse and Williamson (2009) in figure 3. It is seen that the agreement between the model and experiments is very good, which is somewhat surprising due to the absence of the incoming flow velocity in the model. It is also seen that the new formulation gives a much better description of the hydrodynamic damping than the old model (Thorsen et al., 2014a). Based on the results in figures 2 and 3 it is concluded that equation (1) combined with $C_{d,y} = 0.31 + 0.89 y_0/D$ yields a good approximation of the hydrodynamic damping in still water as well as for cross-flow motion at low and high reduced velocities.

The cross-flow excitation and added mass force is modeled according to Thorsen et al. (2015), and the total cross-flow hydrodynamic force is thereby given as:

$$F_y = \frac{1}{2}\rho D U^2 C_v \cos\phi_{\mathrm{exc},y} - \frac{1}{2}\rho D C_{d,y}|\dot{y}|\dot{y} - \rho\frac{\pi D^2}{4}\ddot{y}. \tag{5}$$

The magnitude of the excitation force is determined by the dimensionless coefficient C_v, which is a function of the cross-flow amplitude ratio, y_0/D. The fluctuations of the excitation force due to the vortex shedding process is taken into account through the time variability of the phase $\phi_{\mathrm{exc},y}$, which is coupled to the motion of the cylinder through the equation:

$$\frac{d\phi_{\mathrm{exc},y}}{dt} = H(\phi_{\dot{y}} - \phi_{\mathrm{exc},y}). \tag{6}$$

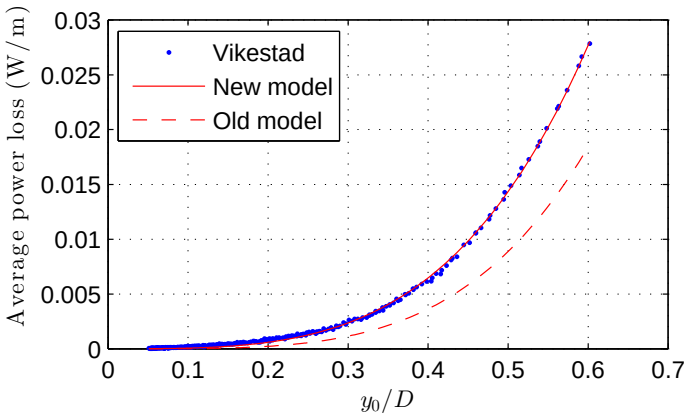

Figure 2: Average power loss (in Watts per unit length of cylinder) due to hydrodynamic damping in still water as a function of non-dimensional vibration amplitude y_0/D. The dots represent the measurements (Vikestad et al., 2000) and the solid line is the present model. The power loss predicted by the old damping model (Thorsen et al., 2014a) is shown with a dashed line.

Here, $\phi_{\dot{y}}$ is the instantaneous phase of the cylinder's cross-flow velocity, and H is a function of $\phi_{\dot{y}} - \phi_{\text{exc},y}$, i.e. the phase difference between the velocity and the excitation force itself. Equation (6) allows the frequency of the force to vary such that the force may synchronize with the velocity of the cylinder, provided that the frequency of motion is within the right range. The function H is shown in figure 4 in non-dimensional frequency form, $\hat{f} = HD/(2\pi U)$. It is seen that the non-dimensional frequency of the excitation force may vary between approximately 0.1 and 0.26, which means that synchronization between the excitation force and motion can occur only if the frequency of motion is within this range.

2.2. Structural model

The elastic cylinder is modeled using finite elements. An example structural model and coordinate system definition is shown in figure 5. Only cross-flow (y-direction) displacements are considered, and the structure is modeled using linear beam elements based on classical beam theory. The stiffening effect from tension is included, such that the element stiffness matrix consists of an elastic (bending) and an initial stress (tension) contribution. The element mass matrix is established using a consistent mass formulation, including both the structural and the hydrodynamic added mass term $0.25\rho\pi D^2$ (see equation 5). Assembling the element contributions, the equation of motion for the structural system reads

$$\mathbf{M}\ddot{\mathbf{r}} + \mathbf{C}\dot{\mathbf{r}} + \mathbf{K}\mathbf{r} = \mathbf{F} \tag{7}$$

where $\mathbf{M}$ is the mass, $\mathbf{C}$ is (structural) damping, $\mathbf{K}$ is stiffness, $\mathbf{F}$ is the hydrodynamic force vector and $\mathbf{r}$ is the structural degrees of freedom. The vector $\mathbf{F}$ is established by evaluating the hydrodynamic force per unit length at the individual nodes (as described in section 2.1, see equation (5)). Note that the added mass term is included in the mass matrix, and not in $\mathbf{F}$. Equation (7) is solved step by step in time domain using the Newmark-β method with coefficients $\gamma = 0.5$ and $\beta = 0.25$. The time step length corresponds to 100 steps per oscillation cycle, based on the expected vibration frequency. This is found to be sufficient, as decreasing the time step size does not affect the results.

2.3. Amplitude estimation

The hydrodynamic excitation and damping forces depend on the amplitude of vibration. This will generally vary along the structure and in time, and must be extracted from the simulated response as the solution progresses. The vibration amplitude at any node is initially calculated as:

$$y_0 = \frac{1}{2}\int_{t_1}^{t_2} |\dot{y}| dt, \tag{8}$$

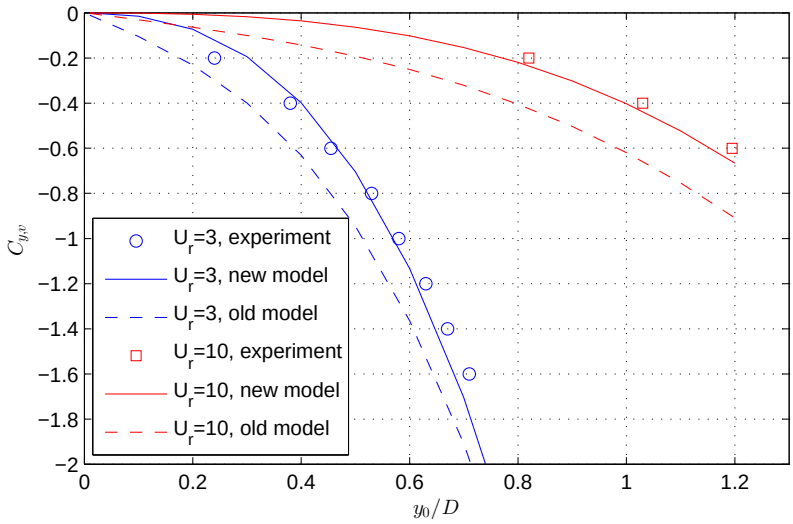

Figure 3: Lift coefficient in phase with cylinder velocity as a function of y_0/D. The circles and squares are from experiments by Morse and Williamson (2009), with $U_r = 3$ and $U_r = 10$ respectively. The corresponding values predicted by the present damping model are shown with solid lines, and the results obtained with the old damping model are shown with dashed lines.

where $\dot{y}$ is the cross-flow velocity of the node, and t_1 and t_2 is the time of the two previous zero-crossings of $\dot{y}$. The rationale behind equation (8) is that the cylinder travels a distance of $2y_0$ in the cross-flow direction between each zero-crossing of $\dot{y}$, assuming that the vibration signal is narrow-banded. A problem with this method is that the amplitude (at a given node) is not a smooth function of time. It can only be updated when a zero-crossing of the velocity occurs, and remains constant between zero-crossings. The sudden change occurring when y_0 is updated may in turn cause a spurious impulse load on the structure, as the hydrodynamic forces change. To overcome this numerical problem, a smoothed amplitude y_0^* is calculated according to the following differential equation:

$$\frac{dy_0^*}{dt} = k_a(y_0 - y_0^*), \tag{9}$$

using $y_0^*(0) = 0$. The smoothed amplitude is then used to evaluate the hydrodynamic coefficients, ensuring that the resulting forces along the structure are smooth, continuous functions of time. The numerical value of k_a determines how rapidly the smoothed amplitude is allowed to change.

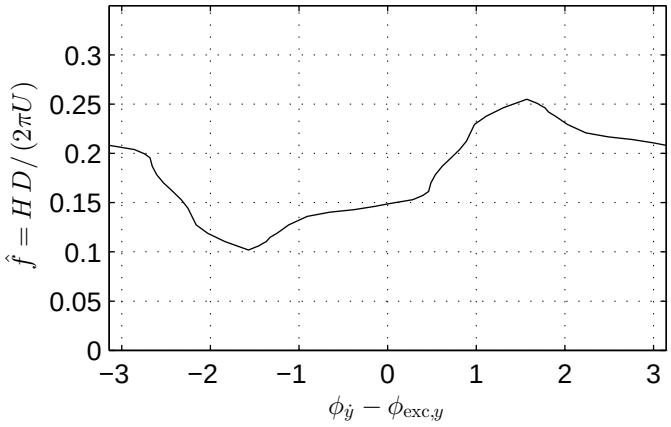

Figure 4: Non-dimensional frequency of the excitation force as a function of the phase difference between the cross-flow velocity and the excitation force.

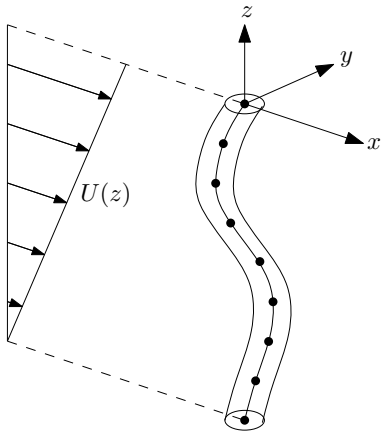

Figure 5: Example of finite element model showing the coordinate system definition and incoming current.

3. Optimizing hydrodynamic excitation force model

In the present hydrodynamic force model, the magnitude of the cross-flow excitation force depends on the dimensionless coefficient C_v, which is a function of the amplitude ratio y_0/D. In the previous papers (Thorsen et al., 2014a,b, 2015), this function was found using the excitation coefficient from the VIVANA database (Larsen et al., 2009). However, a better approach may be to directly utilize data from experiments. Therefore, the strategy used here is to simulate the vortex-induced response of an elastic cylinder in a series of experiments and modify $C_v(y_0/D)$ until the agreement between the simulations and experiments is as good as possible. For this purpose, data from the Norwegian Deepwater Programme (NDP) Riser High Mode VIV tests (Braaten and Lie, 2004; Trim et al., 2005) is utilized. In this experimental campaign, a 38 meter long riser model was towed through the Ocean Basin Laboratory at the Norwegian Marine Technology Research Institute (MARINTEK). The riser was tested in both uniform and sheared flow, where the effective current velocity increased linearly from zero to maximum along the riser length. The maximum velocity was varied from 0.3 m/s to 2.4 m/s. The physical properties of the riser model are given in table 1. The riser was equipped with strain gauges measuring the cross-flow strain at 24 locations along the model, and these measurements are used for comparison with the present model.

It is important to recall that the actual vortex-induced response consists of a fundamental frequency

Table 1: Physical properties of the NDP riser

Length (L)	38 m
Diameter (D)	0.027 m
Mean tension (T)	$4000 - 6000$ N
Bending stiffness (EI)	599 Nm^2
Mass per unit length (m)	0.933 kg/m

component, as well as higher harmonic frequencies (Vandiver et al., 2006; Modarres-Sadeghi et al., 2010). As the model includes only the fundamental frequency response, the higher harmonic components in the experimental data are removed by filtering, such that the simulations are compared to the measured fundamental frequency response only. An example of the measured cross-flow strain before and after removing the higher harmonic components is shown in figure 6. To quantify the prediction error for a given measurement, the maximum value of the root-mean-square (r.m.s.) of strain in each test is used. Thereby, the prediction error for a specific test is

$$e_i = \hat{\sigma}_{\max,i} - \sigma_{\max,i}, \tag{10}$$

where $\sigma_{\max,i}$ is the maximum r.m.s. of strain in test number i, and $\hat{\sigma}_{\max,i}$ is the corresponding prediction.

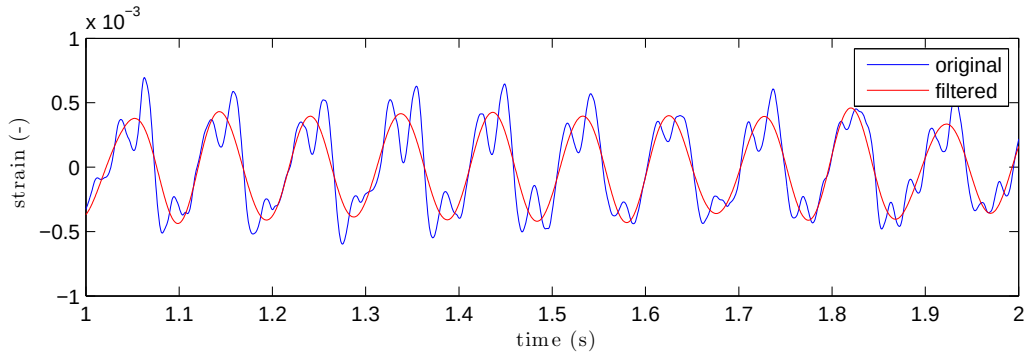

Figure 6: Example of measured strain before and after removal of higher harmonic components. The time series is from a uniform flow test with $U = 2.0$ m/s, measured at the position of maximum r.m.s. strain.

To find the best possible $C_v(y_0/D)$, the curve is parametrized such that the problem is reduced to finding the optimal set of parameters. The parameters are the coordinates of the maximum point (p_1) and the zero-crossing point (p_2). Between the specified points, the curve is described by second order polynomials. It is also assumed that $C_v(y_0/D)$ is either positive or zero (not negative). An optimization task may then be formulated, where the goal is to minimize the sum of the square errors, $\sum e_i^2$. This is done by simulating all the test cases (22 uniform and 22 sheared flow tests), and systematically varying the coordinates of p_1 and p_2 until the minimum error sum is found. The MATLAB implementation of the Nelder-Mead simplex method (Lagarias et al., 1998) is used to search for the optimal parameters. The curve which is found to provide the minimum prediction error is shown in figure 7, and the predicted maximum r.m.s. of the cross-flow strain is compared to the measurements in figure 8a (uniform flow) and 8b (sheared flow). The maximum r.m.s. of the measured total strain (including higher harmonics) is also shown for comparison.

With reference to figures 8a and 8b it is evident that the model is not perfect, even though an optimal excitation curve has been applied. The optimization of $C_v(y_0/D)$ was performed considering 44 cases simultaneously, but the resulting curve is not necessarily the best for each case. This suggests that the underlying physical process may be viewed as stochastic, such that the optimal excitation curve found here represents an average, or expected value of $C_v(y_0/D)$. However, considering the simple formulation of the model and the complicated problem at hand, the overall agreement is satisfactory. To illustrate more

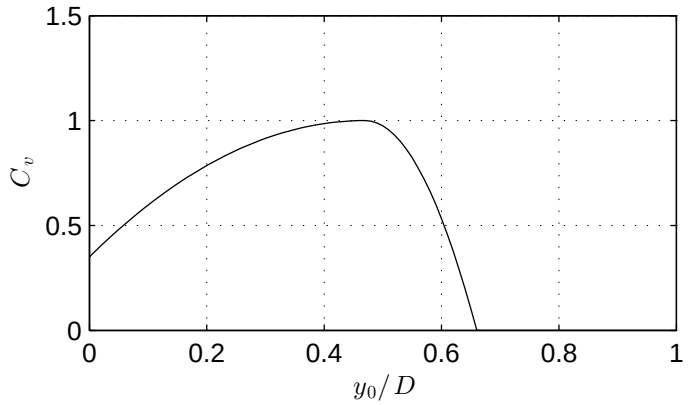

Figure 7: Optimal C_v as a function of y_0/D.

thoroughly how the model performs, the r.m.s. of the cross-flow strain along the riser is shown for three selected cases in figure 9 (uniform flow) and 10 (sheared flow). The spectrum of the measured and simulated strain (at the location of the maximum r.m.s. of strain) is also shown. It is seen that the measurements contain higher harmonics around 3 times the fundamental frequency. These are not included in the model, but the fundamental frequency is predicted with good accuracy.

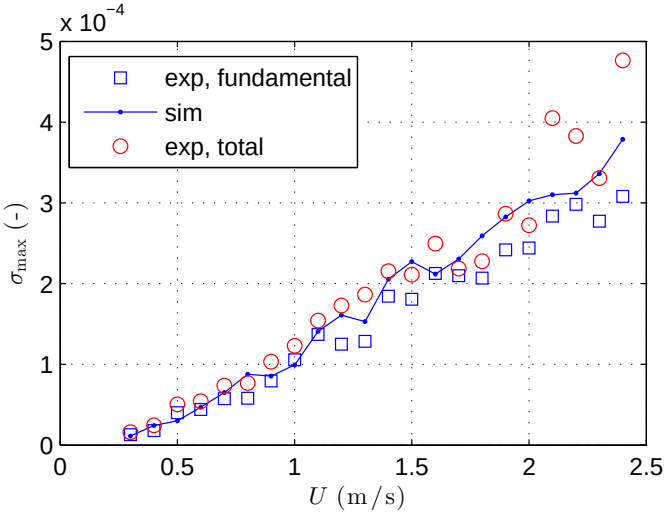

(a) Uniform flow

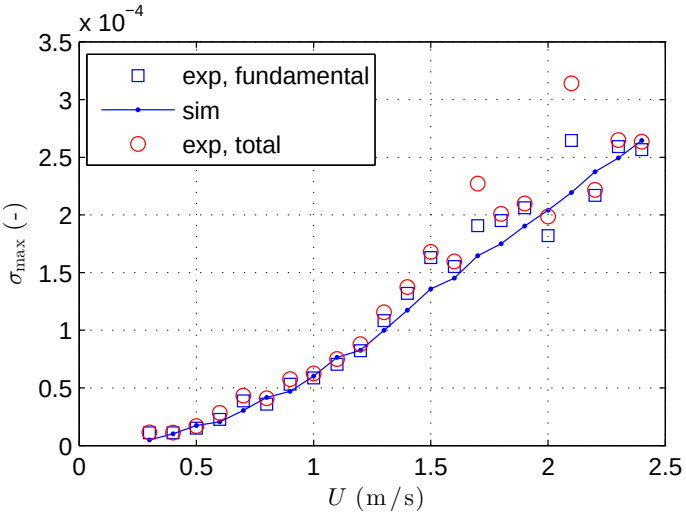

(b) Sheared flow

Figure 8: Maximum r.m.s. of cross-flow strain for all cases included in the optimization, shown as a function of the incoming flow velocity (for shear flow, U is the maximum flow velocity). The results based on measured total strain are shown as circles and those based on fundamental frequency strain as squares. The simulated results are shown as dots connected with a solid line.

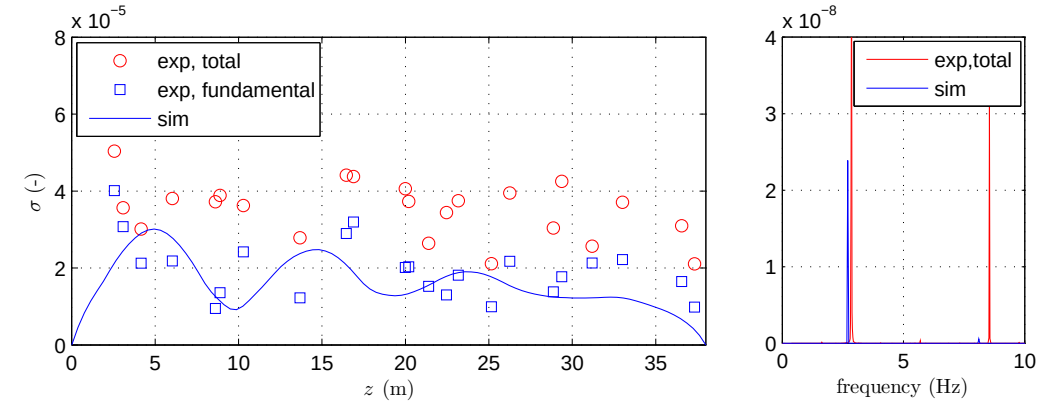

(a) $U = 0.5\,\mathrm{m/s}$

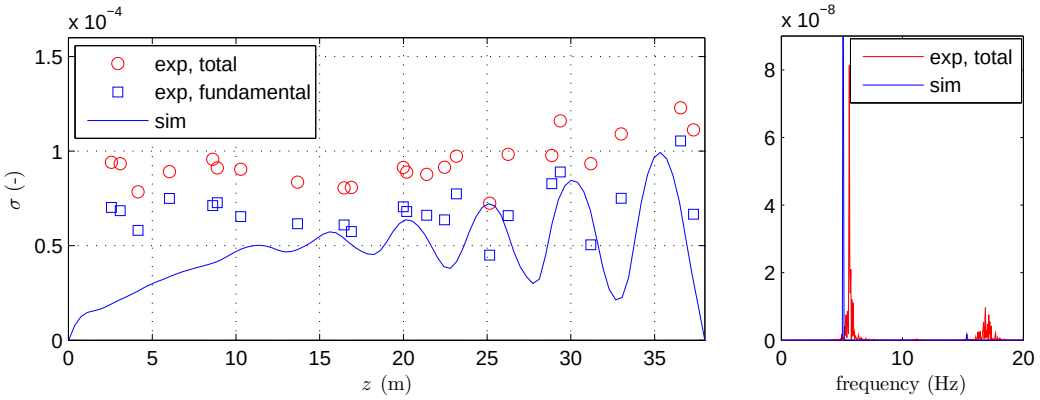

(b) $U = 1.0\,\mathrm{m/s}$

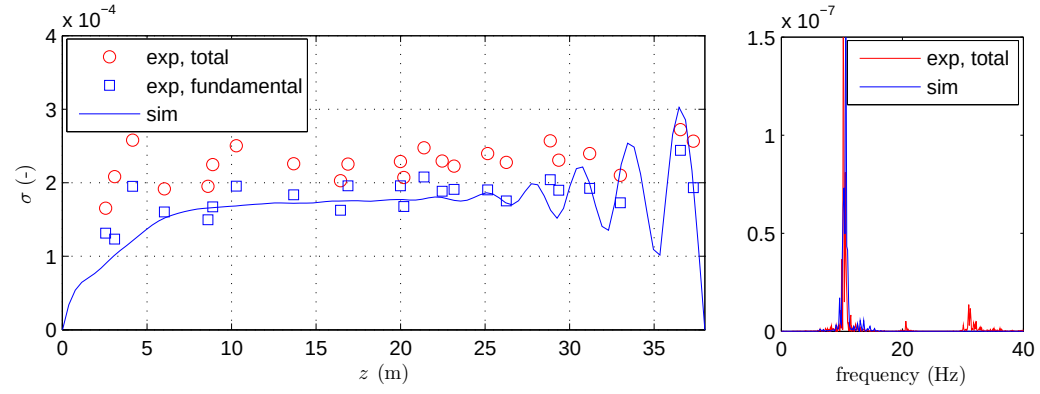

(c) $U = 2.0\,\mathrm{m/s}$

Figure 9: Uniform flow results: To the left is the r.m.s. of cross-flow strain along the riser for three different cases. Red circles: total measured strain, blue squares: measured fundamental frequency strain, solid line: strain from simulation. To the right is the power spectrum of cross-flow strain at the location of maximum r.m.s. strain. Red is measured and blue is simulated.

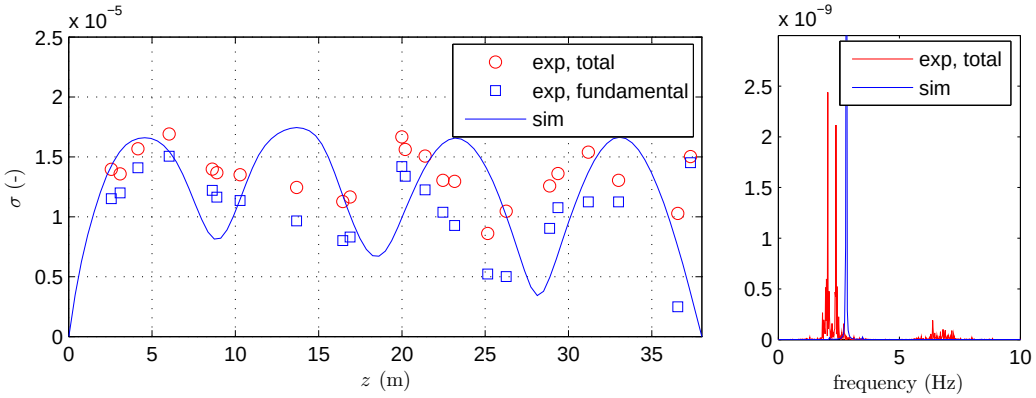

(a) $U = 0.5\,\mathrm{m/s}$

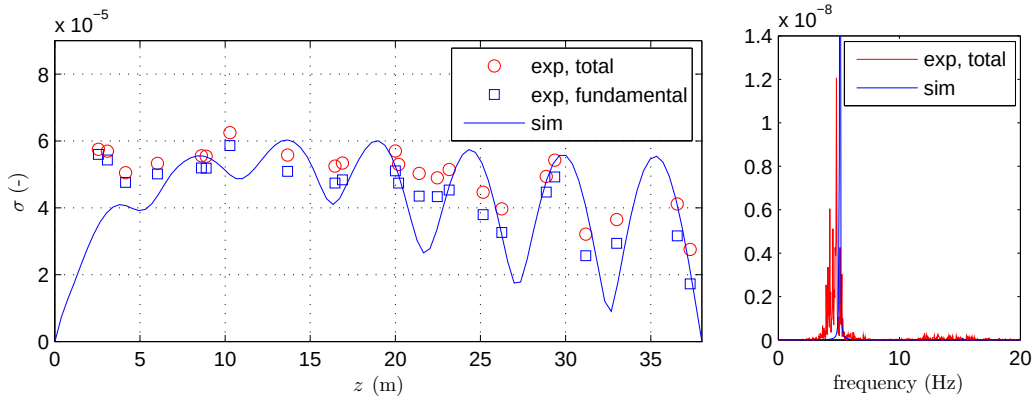

(b) $U = 1.0\,\mathrm{m/s}$

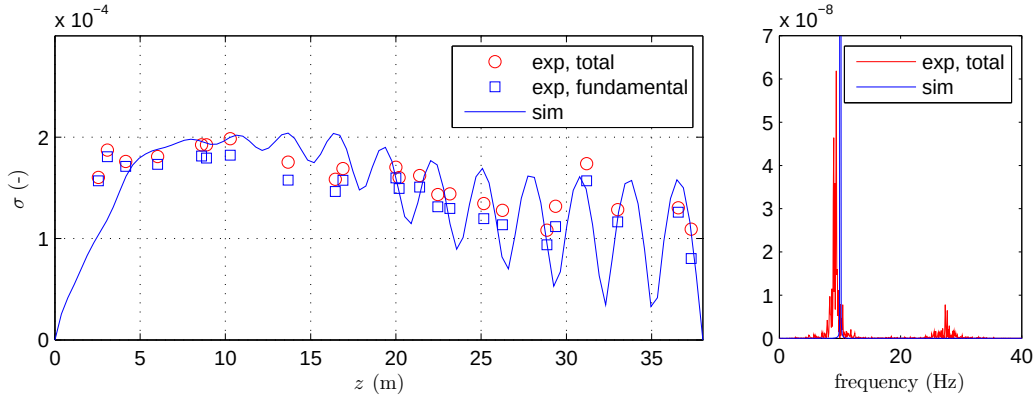

(c) $U = 2.0\,\mathrm{m/s}$

Figure 10: Sheared flow results: To the left is the r.m.s. of cross-flow strain along the riser for three different cases. Red circles: total measured strain, blue squares: measured fundamental frequency strain, solid line: strain from simulation. To the right is the power spectrum of cross-flow strain at the location of maximum r.m.s. strain. Red is measured and blue is simulated.

4. Flexible cylinder in oscillating flow

4.1. Overview

An experimental investigation of VIV in oscillating flow was performed by Fu et al. (2014). These experiments were conducted in the ocean basin at Shanghai Jiao Tong University (SJTU), and consisted of a flexible cylinder being towed horizontally with a prescribed oscillating motion. The oscillation amplitude and period was varied, such that the cylinder experienced oscillating flow with different combinations of KC numbers and maximum reduced velocities, $U_{r,\max}$. Denoting the amplitude of the prescribed oscillating motion as A_m, the KC number may be defined as

$$\mathrm{KC} = \frac{U_{\max} T}{D} = \frac{2\pi A_m}{D}, \tag{11}$$

where $U_{\max}$ is the maximum velocity of the incoming oscillating flow and T is the corresponding period. The maximum reduced velocity may then be expressed as

$$U_{r,\max} = \frac{U_{\max}}{f_1 D} = \frac{2\pi A_m}{T f_1 D} = \frac{\mathrm{KC}}{T f_1}, \tag{12}$$

where f_1 is the lowest natural frequency of the cylinder in still water. Key properties of the test cylinder are given in table 2, and a simplified overview of the experimental set up is shown in figure 11. At both ends, the cylinder was attached to universal joints, allowing free rotation around the x- and y-axis (ref. figure 5). A large number of cases were included in the experiments, with KC numbers between 26 and 178 and maximum reduced velocities between 4 and 7.9. The model was equipped with strain gauges measuring the cross-flow strain at 7 equally spaced positions along the length. As only lower modes (mode 1-2) were excited, the number of measuring points are sufficient to perform modal reconstruction of the displacements, as described by e.g. Lie and Kaasen (2006).

Table 2: Physical properties of the test cylinder

Length, L	4 m
Diameter, D	0.024 m
Mass per unit length, m	0.69 kg/m
Mass ratio, $m/(0.25\rho\pi D^2)$	1.53
Bending stiffness, EI	10.5 Nm^2
Pretension, T	500 N
Structural damping (in air)	1.5 %

4.2. Simulation and comparison with experiment

To test how the present simulation model performs at predicting VIV in oscillating flows, the model is used to recreate the SJTU experiments. Some simplifications are introduced: The small displacements due to mean drag and weight are neglected. Furthermore, the oscillatory motion is transformed to an oscillating incoming current, meaning that the boundary conditions of the model is zero displacement (but free rotation) at both ends. This is possible because the inertial forces associated with the oscillatory motion are small compared to the vortex-induced forces. In addition, the small fluctuations in tension are neglected and a constant $T = 500\,\mathrm{N}$ is used. Recall that the model was tuned to stationary flow measurements, and no changes in the hydrodynamic modeling are introduced. The results will therefore clearly show whether or not it is reasonable to predict VIV in oscillating flow based on data from stationary flow VIV.

To investigate the model performance at different KC numbers and reduced velocities, four cases are considered as shown in table 3. In Case 1 and 2 the KC number is low, meaning the cylinder travels a relatively short distance in one direction, before it turns back into its own wake. Hence it is expected that previously shed vortices are still present in the wake, which will affect the lift force on the cylinder. Also,

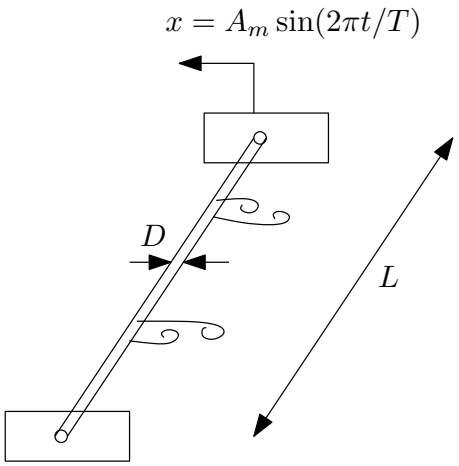

Figure 11: Simplified overview of the SJTU experimental set up.

the number of generated vortices per flow period is low. In case 3 and 4 the KC number is increased to 178. In these cases, the cylinder travels significantly longer between each flow reversal, meaning the situation is more similar to a steady flow. In addition, different values of the reduced velocity are considered. The higher value ($U_r = 6.5$) corresponds to the point where the maximum vibration amplitude is expected, based on stationary flow observations (see e.g. Sumer and Fredsøe (1997)). The lower value is included to see how the model performs when the lock-in situation is less perfect.

Table 3: Test cases used for comparison.

Case No.	A_m	T	KC	$U_{r,\max}$
1	0.12 m	2.5 s	31.4	4.7
2	0.12 m	1.8 s	31.4	6.5
3	0.68 m	16.5 s	178	4.0
4	0.68 m	10.2 s	178	6.5

The simulation results are shown in figures 12-15 together with the corresponding experimental results. Starting with case 1, it is seen that the cylinder vibrates at mode 1, i.e. one half-wave along the cylinder span. The measured response consists mainly of a single dominating frequency component at approximately 2.5 Hz, but lower frequencies are also present, causing the overall response to appear slightly irregular. The simulated response is more regular, but the dominating frequency and amplitude is well captured. Due to the low KC number, there is not much time for the vibration amplitude to diminish between periods with high flow velocity. Therefore, the response appears almost stationary, which is also seen in the simulation.

For case 2, the response is similar to case 1, but the amplitude is larger as a result of the increased reduced velocity. As the reduced velocity is close to the ideal value for synchronization between the vortex shedding and the natural frequency of the structure, the measured response is more regular than in case 1, and contains essentially only a single frequency component around 2.8 Hz. This is also seen in the simulations, which reproduces both the amplitude and frequency with good accuracy. Again, the response is almost stationary in time, as the flow velocity increases to a level sufficiently high for positive power transfer between the fluid and structure, before the vibration amplitude has decreased notably.

Moving on to case 3, the effect of increasing the KC number is clearly illustrated. The flow velocity now changes slowly compared to the vibration frequency, causing the amplitude to decay significantly during periods of low incoming flow velocity. This is seen both in the experiment and the simulation. The frequency and amplitude are rather accurately predicted, although the amplitude is slightly larger than measured. The building-up and dying-out effect is realistically reproduced in the simulations.

In case 4, the KC number is the same as for case 3, but the maximum reduced velocity is closer to the point of maximum vibration amplitude. This means the incoming flow velocity is large enough to cause positive excitation a larger fraction of the time. It is seen that as the flow velocity increases, the vibration amplitude builds up rapidly, before a maximum value is reached. The vibration continues at this constant amplitude for some time, before the flow velocity reduces to a level where vortex shedding no longer can excite the structure. The ongoing process of "building-up", "lock-in" and "dying out" was described by Fu et al. (2014), and is clearly seen in both the experiment and simulation. An interesting feature is that the amplitude builds up faster than it decays, which is also captured by the model.

To summarize the comparison in figures 12-15, it has been shown that the model is able to predict cross-flow VIV of a flexible cylinder for KC numbers 31 and 178. For KC = 31, the number of vortex shedding periods between flow reversals is low, approximately 3. Hence, one would expect the incoming flow to be significantly disturbed by previously shed vortices. It is therefore somewhat surprising that the simulations are seen to reproduce the observed behavior quite accurately, even though the hydrodynamic force model was initially adjusted according to data from stationary flow VIV experiments. This suggests that the effect of the disturbed incoming flow is small (at least for the KC numbers considered here), and that the relevant hydrodynamic forces can be found using the same mathematical description as in stationary flows, if the time variability of the incoming flow velocity is taken properly into account.

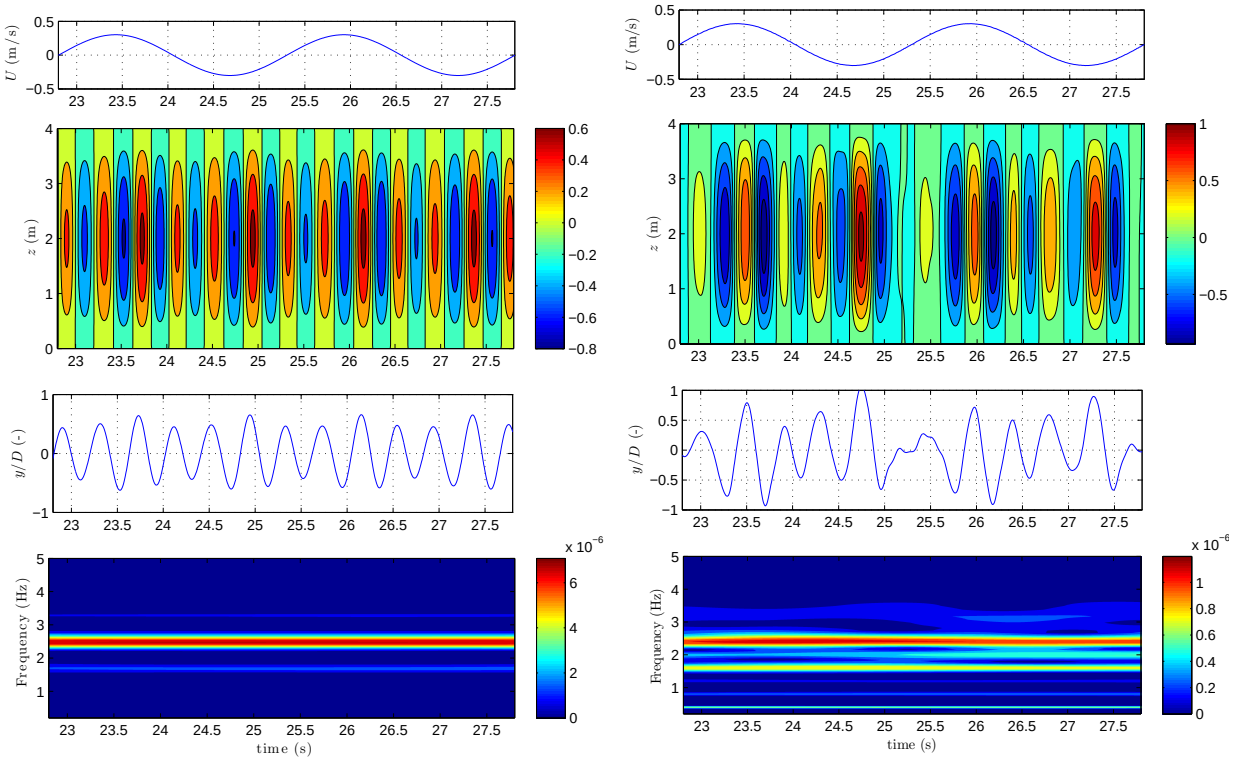

(a) Simulation

(b) Experiment

Figure 12: Case 1 results. The top row shows the incoming current velocity U as a function of time. The row below shows the normalized cross-flow displacement y/D in time and space. The next row shows y/D at the mid-span, i.e. at $z = 2\,\mathrm{m}$. At the bottom is a wavelet contour plot of the vibration energy at the mid-span, showing the frequency content over time.

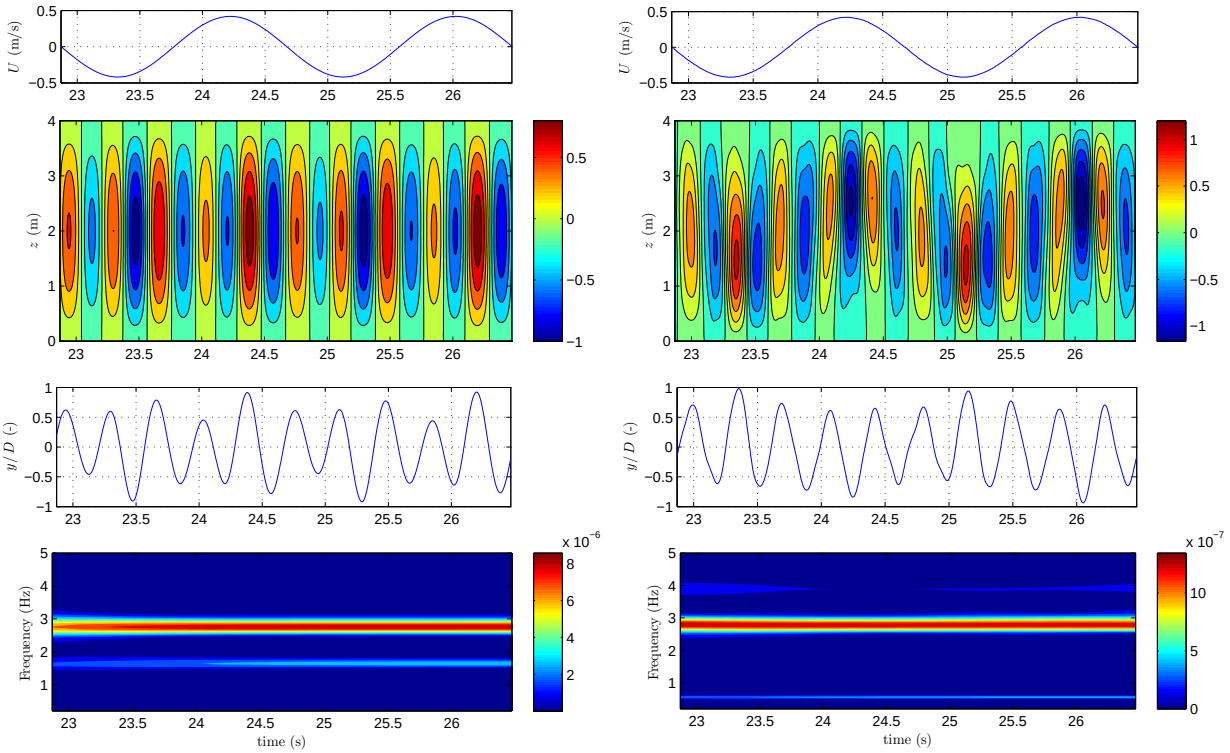

(a) Simulation

(b) Experiment

Figure 13: Case 2 results. The top row shows the incoming current velocity U as a function of time. The row below shows the normalized cross-flow displacement y/D in time and space. The next row shows y/D at the mid-span, i.e. at $z = 2\,\mathrm{m}$. At the bottom is a wavelet contour plot of the vibration energy at the mid-span, showing the frequency content over time.

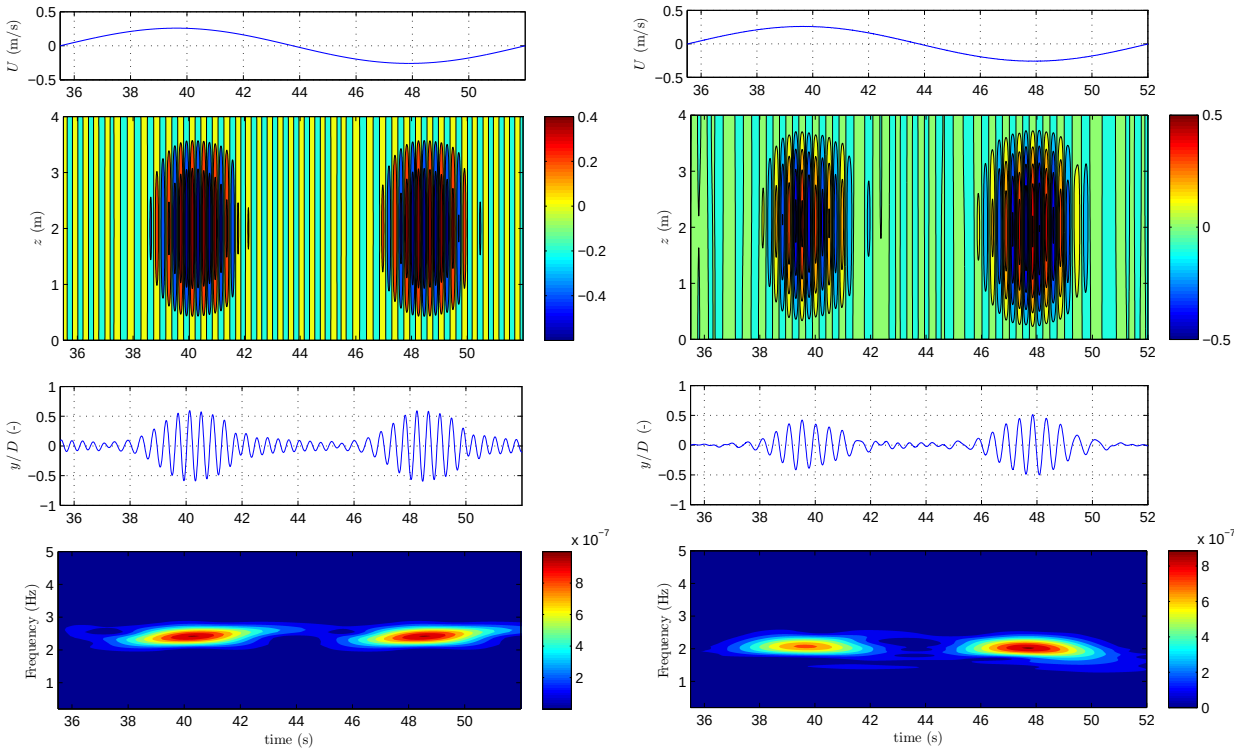

(a) Simulation

(b) Experiment

Figure 14: Case 3 results. The top row shows the incoming current velocity U as a function of time. The row below shows the normalized cross-flow displacement y/D in time and space. The next row shows y/D at the mid-span, i.e. at $z = 2\,\mathrm{m}$. At the bottom is a wavelet contour plot of the vibration energy at the mid-span, showing the frequency content over time.

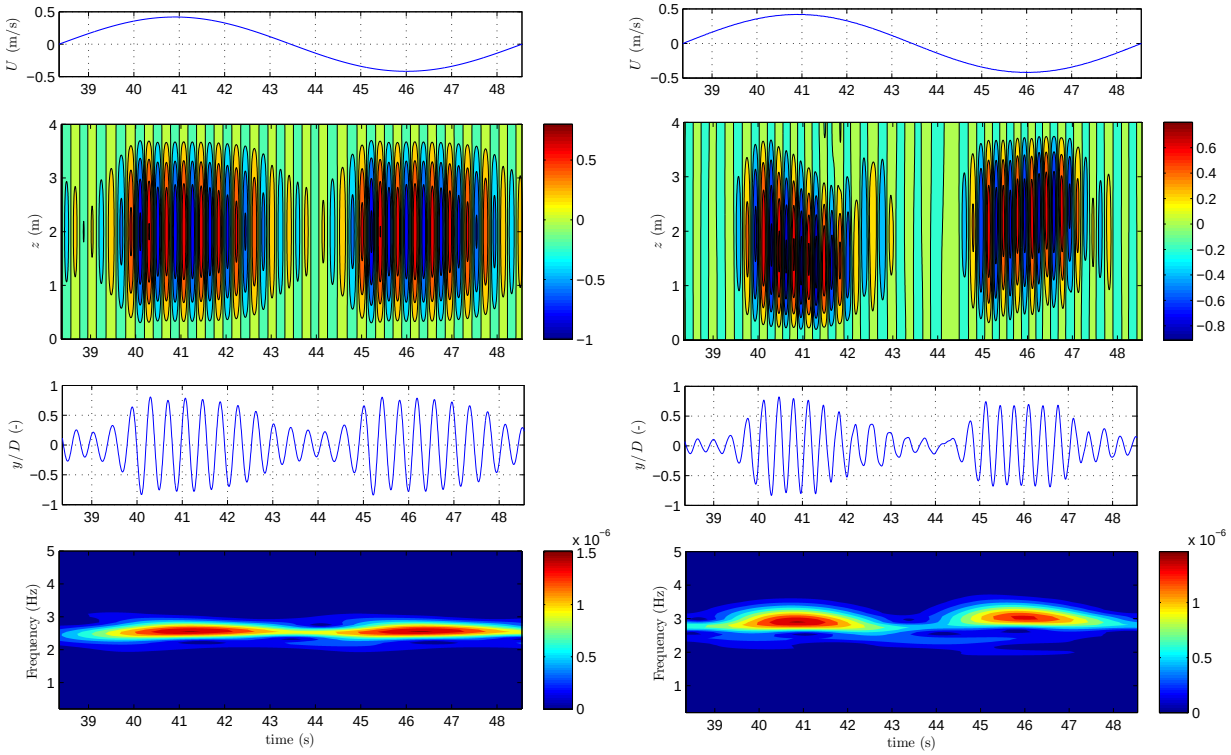

(a) Simulation

(b) Experiment

Figure 15: Case 4 results. The top row shows the incoming current velocity U as a function of time. The row below shows the normalized cross-flow displacement y/D in time and space. The next row shows y/D at the mid-span, i.e. at $z = 2\,\mathrm{m}$. At the bottom is a wavelet contour plot of the vibration energy at the mid-span, showing the frequency content over time.

4.3. Effect of reduced velocity and mass ratio

The comparison in the previous section indicates that the hydrodynamic force model includes the most relevant physical effects, and it is therefore fair to assume that this remains true when external parameters such as incoming flow velocity and structural mass are changed. In the experiments by Fu et al. (2014), the magnitude of the relative flow velocity was such that mainly the first natural mode of the structure was excited by vortex shedding (some participation of mode 2 was also seen). Increasing the velocity further could reveal some interesting phenomena. For instance, if the maximum flow velocity corresponds to excitation of a high mode, then a number of lower modes may be excited before the maximum flow velocity is reached. In such cases it is not clear how the response will look like, and the present model is utilized to investigate this.

4.3.1. Example 1: High reduced velocity

The KC number and other parameters are the same as in the previously shown case 3 and 4, except the maximum reduced velocity, which is increased to $U_{r,\max} = 32$ to excite higher modes of vibration. Before moving on to the simulation results, it is illustrated how the expected excitation frequency varies with time, due to the oscillating flow velocity. A simple way to estimate the excitation frequency would be to assume a constant non-dimensional frequency, and according to experiments (Gopalkrishnan, 1993), the energy transfer is largest around $\hat{f} = fD/U \approx 0.17$. Hence, the expected vibration frequency can be found from the instantaneous flow velocity as $f(t) = 0.17|U(t)|/D$. This is shown in figure 16, where the 5 first natural frequencies of the structure (in still water) are shown with dashed lines. As the flow velocity increases, it is seen that the expected vibration frequency passes the three lowest natural frequencies, and finally exceeds the fourth before it starts reducing. Hence one would expect the response to consist of modes 1-4.

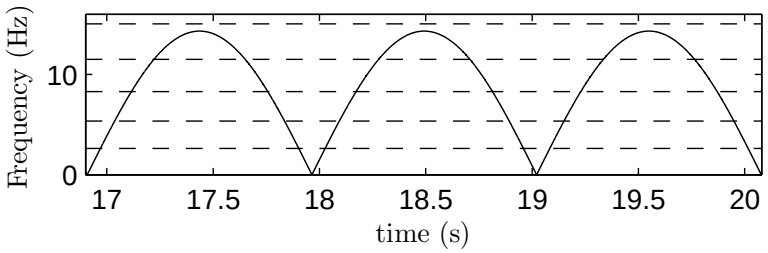

Figure 16: Expected vibration frequency, $f = 0.17|U|/D$, as a function of time (solid line). The dashed lines are the first 5 natural frequencies of the cylinder.

The simulation results are shown in figure 17. The complex pattern resulting from the continuously changing mode and frequency is easily seen. The modal weight factors $w_n(t)$ for the first 5 modes are also shown, giving a clearer picture of how the dominating mode varies with time. The modal weights are related to the cross-flow displacement through the following equation:

$$y(z,t) = \sum_{n=1}^{\infty} w_n(t)\psi_n(z) = \sum_{n=1}^{\infty} w_n(t)\sin(n\pi z/L). \tag{13}$$

As seen in figure 17, mode 1 dominates in periods of low flow velocity. When the velocity increases, a transition to mode 3 is seen, before mode 4 finally takes over. When the velocity has decreased sufficiently, mode 3 and 4 dies out, and mode 1 starts to dominate once more. It is also seen that each oscillation cycle (from one flow reversal to the next) is slightly different from the previous, meaning the response is not periodic. Because the duration of one flow cycle is short relative to the first natural frequency, the response at mode 1 does not have time to decay significantly, even when the flow velocity is too high to excite this mode. Hence, the response in periods with high flow velocity is a superposition of the previously activated mode 1 together with mode 3 or 4 which is currently being excited. This causes the maximum cross-flow displacement to become somewhat larger than in the previously considered cases containing only mode 1.

4.3.2. Example 2: High reduced velocity combined with high mass ratio

The mass ratio $m^* = m/(0.25\rho\pi D^2)$ of the cylinder studied by Fu et al. (2014) was 1.53. As mass ratio is identified as one of the dimensionless parameters important to the VIV response of cylinders in stationary flow (Williamson and Govardhan, 2004), it is of interest to investigate how this parameter affects VIV in oscillating flows. With this in mind, another simulation is performed, where the mass of the cylinder is increased by a factor of 5. This gives a mass ratio of 7.65, corresponding to a solid steel cylinder. The KC number and maximum reduced velocity are kept the same as in example 1, meaning that the flow may still potentially excite modes 1-4, as illustrated in figure 16 (although the numerical values of the frequencies are changed due to the increased mass).

The simulation results are shown in figure 18. In comparison to the low mass ratio case, the response appears less complicated. The cross-flow displacement is almost single-moded with mode 3 clearly dominating. The amplitude varies only slightly, with maximum values occurring around the time of maximum flow velocity, and minimum values when U is close to zero. The frequency content as seen in the wavelet contour plot is nearly constant in time, with the energy concentrated around 4.7 Hz, which is close to the 3rd natural frequency. The maximum vibration amplitude is smaller than in the previous example, and the maximum y/D is approximately 0.7. These results, and particularly the differences between example 1 and 2 can be qualitatively explained as follows. Due to the increased mass and inertia, the cylinder is more resistant to change in the vibration state, and therefore continues at the same mode and frequency even when this is no longer being excited by vortex shedding. Furthermore, as the vibration frequency is almost constant, there will be periods of time when the vortex shedding is unable to synchronize with the cylinder motion, and the energy transfer from fluid to structure will hence be reduced compared to example 1. This explains why the maximum vibration amplitude is smaller for the high mass ratio case.

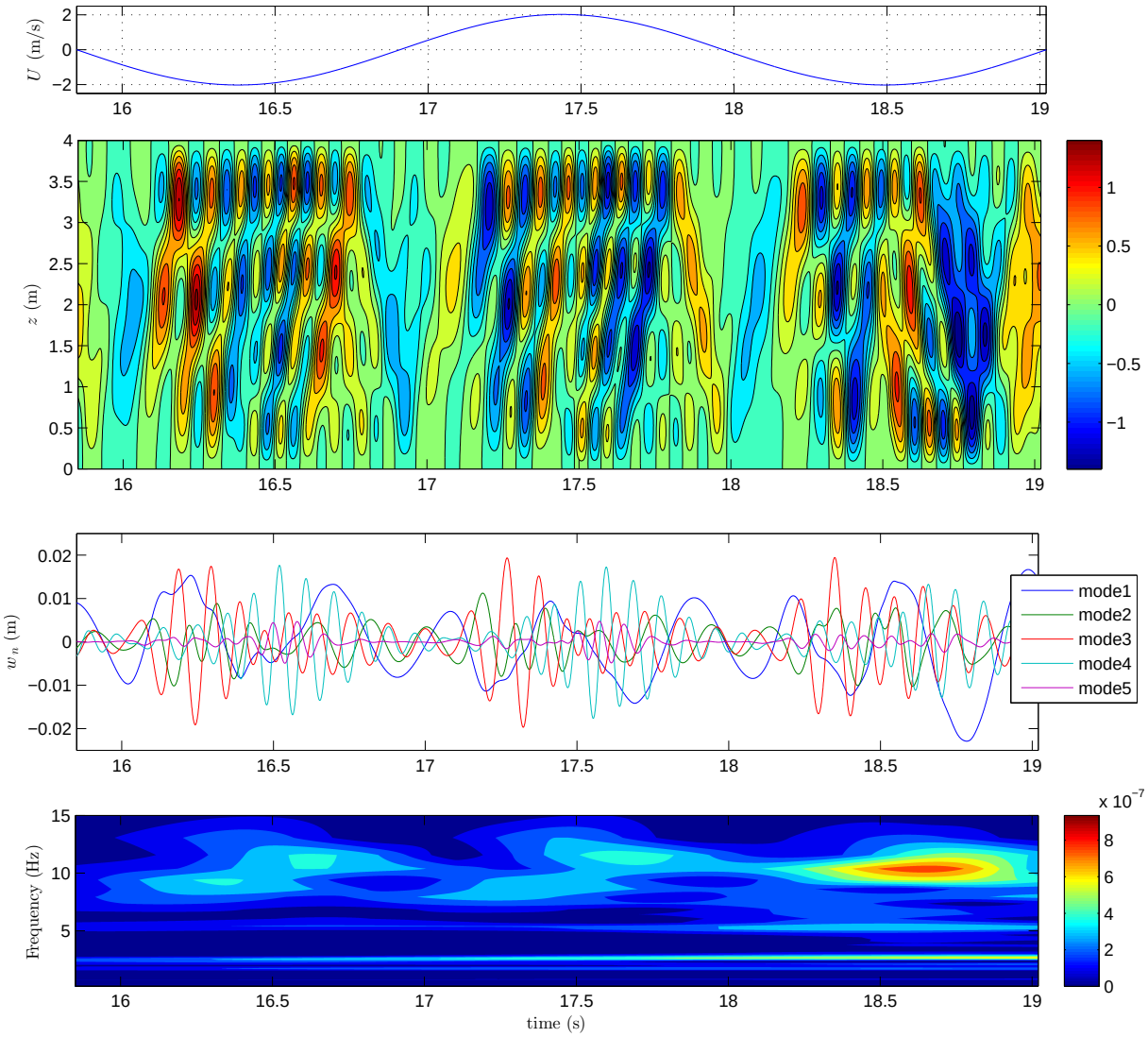

Figure 17: Simulation results for example 1. At the top: incoming flow velocity U as a function of time. Below is a contour plot of the normalized cross-flow displacement y/D in time and space. The next figure shows the modal weight factors, $w_n(t)$, for mode 1 to 5. At the bottom is the wavelet contour plot of the energy-density of the cross-flow displacement at $z = 0.5\,\mathrm{m}$.

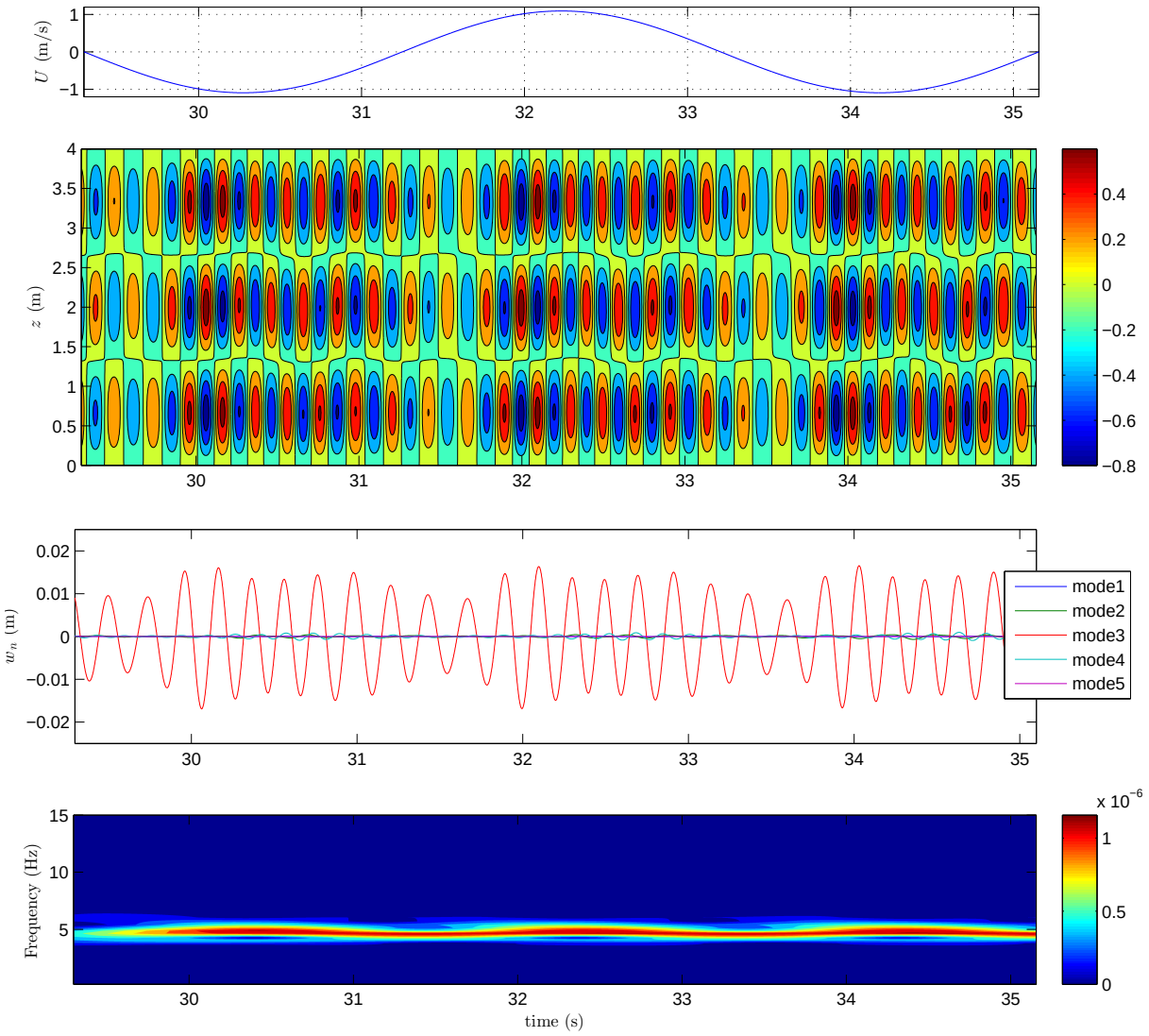

Figure 18: Simulation results for example 2. At the top: incoming flow velocity U as a function of time. Below is a contour plot of the normalized cross-flow displacement y/D in time and space. The next figure shows the modal weight factors, $w_n(t)$, for mode 1 to 5. At the bottom is the wavelet contour plot of the energy-density of the cross-flow displacement at $z = 0.5\,\mathrm{m}$.

5. Conclusions

The hydrodynamic force model developed by Thorsen et al. (2014a) has been improved by introducing a new damping formulation, with parameters obtained from experimental data. It is demonstrated that the predicted damping corresponds well with actual measurements in still water and for cross-flow oscillations in stationary flow at low and high reduced velocity. Furthermore, the excitation force model is optimized through comparison with a series of tests with a flexible cylinder in uniform and sheared flow. In these tests, the incoming flow was stationary, meaning that no information from VIV in oscillating flow was used to construct the hydrodynamic force model.

The optimized model was used to simulate the cross-flow VIV of an elastic cylinder in oscillating flow at different KC numbers and maximum reduced velocities. Comparison with experiments shows that the model provides realistic results in terms of important characteristics such as frequency content, mode and amplitude of vibration. For high KC numbers, the vibrations continuously build up and die out, which is well captured by the simulations. This indicates that the relevant hydrodynamic forces in oscillating flow can be found from empirical relationships obtained from experiments in stationary flow, at least for the KC numbers considered in this study (31 and 178).

The model was also used to investigate the effect of increasing the maximum reduced velocity and mass ratio of the flexible cylinder. When $U_{r,\max} = 32$ and $m^* = 1.53$, the dominating mode and frequency changes continuously as the vortex shedding excites different natural frequencies depending on the velocity of the incoming flow. This results in the appearance of a complex response pattern. In contrast, when the mass ratio is increased by a factor of 5, the response is almost stationary with a single dominating mode. A possible explanation is that the heavy cylinder is more resistant to change in the vibration state due to the larger inertia.

Acknowledgments

The authors would like to thank Statoil for permission to use the data from the oscillating flow experiments performed at Shanghai Jiao Tong University. We are also very grateful to the Norwegian Deepwater Programme (NDP) Riser and Mooring Project for permission to use the Riser High Mode VIV test data. Finally, we would like to thank Jungao Wang for sharing his experience on VIV in oscillating flows and Jie Wu for providing help with the wavelet analysis.

References

Aglen, I. M., Larsen, C. M., 2011. Importance of added mass for the interaction between IL and CF vibrations of free spanning pipelines. In: ASME 2011 30th International Conference on Ocean, Offshore and Arctic Engineering. American Society of Mechanical Engineers, pp. 545–556.

Bearman, P., 2011. Circular cylinder wakes and vortex-induced vibrations. Journal of Fluids and Structures 27 (5–6), 648 – 658.

Blevins, R. D., 1990. Flow-Induced Vibration, 2nd Edition. Van Nostrand Reinhold.

Braaten, H., Lie, H., 2004. NDP riser high mode VIV tests, main report. Tech. rep., Norwegian Marine Technology Research Institute, Trondheim, Norway.

Chang, S.-H. M., Isherwood, M., et al., 2003. Vortex-induced vibrations of steel catenary risers and steel offloading lines due to platform heave motions. In: Offshore Technology Conference. Offshore Technology Conference.

Chaplin, J., Bearman, P., Huera Huarte, F., Pattenden, R., 2005. Laboratory measurements of vortex-induced vibrations of a vertical tension riser in a stepped current. Journal of Fluids and Structures 21 (1), 3–24.

Feng, C., 1968. The measurement of vortex induced effects in flow past stationary and oscillating circular and D-section cylinders. Master's thesis, University of British Columbia.

Fu, S., Wang, J., Baarholm, R., Wu, J., Larsen, C., 2014. Features of vortex-induced vibration in oscillatory flow. Journal of Offshore Mechanics and Arctic Engineering 136 (1), 011801.

Gopalkrishnan, R., 1993. Vortex-induced forces on oscillating bluff cylinders. Ph.D. thesis, Massachusetts Institute of Technology.

Govardhan, R., Williamson, C., 2000. Modes of vortex formation and frequency response of a freely vibrating cylinder. Journal of Fluid Mechanics 420 (85), 130.

Huera-Huarte, F., Bangash, Z., González, L., 2014. Towing tank experiments on the vortex-induced vibrations of low mass ratio long flexible cylinders. Journal of Fluids and Structures 48, 81–92.

Huse, E., Kleiven, G., Nielsen, F., et al., 1998. Large scale model testing of deep sea risers. In: Offshore Technology Conference.
Jauvtis, N., Williamson, C., 2004. The effect of two degrees of freedom on vortex-induced vibration at low mass and damping. Journal of Fluid Mechanics 509 (6), 23–62.
Lagarias, J. C., Reeds, J. A., Wright, M. H., Wright, P. E., 1998. Convergence properties of the Nelder–Mead simplex method in low dimensions. SIAM Journal on optimization 9 (1), 112–147.
Larsen, C. M., Lie, H., Passano, E., Yttervik, R., Wu, J., Baarholm, G., 2009. VIVANA - Theory Manual, Version 3.7.
Liao, J.-C., 2001. Vortex-induced vibration of slender structures in unsteady flow. Ph.D. thesis, Massachusetts Institute of Technology.
Lie, H., Kaasen, K., 2006. Modal analysis of measurements from a large-scale VIV model test of a riser in linearly sheared flow. Journal of Fluids and Structures 22 (4), 557–575.
Modarres-Sadeghi, Y., Mukundan, H., Dahl, J., Hover, F., Triantafyllou, M., 2010. The effect of higher harmonic forces on fatigue life of marine risers. Journal of Sound and Vibration 329 (1), 43–55.
Moe, G., Wu, Z.-J., 1990. The lift force on a cylinder vibrating in a current. Journal of Offshore Mechanics and Arctic Engineering 112 (4), 297–303.
Morse, T., Williamson, C., 2009. Prediction of vortex-induced vibration response by employing controlled motion. Journal of Fluid Mechanics 634, 5–39.
Norberg, C., 2003. Fluctuating lift on a circular cylinder: review and new measurements. Journal of Fluids and Structures 17 (1), 57–96.
Resvanis, T. L., 2014. Vortex-induced vibration of flexible cylinders in time-varying flows. Ph.D. thesis, Massachusetts Institute of Technology.
Sarpkaya, T., 1978. Fluid forces on oscillating cylinders. NASA STI/Recon Technical Report A 78, 46523.
Sarpkaya, T., 1979. Lateral oscillations of smooth and sand-roughened cylinders in harmonic flow. Mechanics of Wave-Induced Forces on Cylinders (ed. TL Shaw), Pitman, London, 421–435.
Sarpkaya, T., 1986. Force on a circular cylinder in viscous oscillatory flow at low keulegan—carpenter numbers. Journal of Fluid Mechanics 165, 61–71.
Sarpkaya, T., 2004. A critical review of the intrinsic nature of vortex-induced vibrations. Journal of Fluids and Structures 19 (4), 389 – 447.
Sarpkaya, T., 2010. Wave forces on offshore structures. Cambridge University Press.
Sumer, B., Fredsøe, J., 1988. Transverse vibrations of an elastically mounted cylinder exposed to an oscillating flow. Journal of Offshore Mechanics and Arctic Engineering 110 (4), 387–394.
Sumer, B. M., Fredsøe, J., 1997. Hydrodynamics around cylindrical structures. Vol. 12. World Scientific Publishing Company.
Thorsen, M., Sævik, S., Larsen, C., 2015. Fatigue damage from time domain simulation of combined in-line and cross-flow vortex-induced vibrations. Marine Structures 41, 200–222.
Thorsen, M., Sævik, S., Larsen, C., 2014a. A simplified method for time domain simulation of cross-flow vortex-induced vibrations. Journal of Fluids and Structures.
Thorsen, M., Sævik, S., Larsen, C., 2014b. Time domain simulation of cross-flow and in-line vortex-induced vibrations. In: Proceedings of EURODYN 2014. Porto, Portugal.
Triantafyllou, M., Triantafyllou, G., Tein, Y., Ambrose, B. D., et al., 1999. Pragmatic riser VIV analysis. In: Offshore Technology Conference. Offshore Technology Conference.
Trim, A., Braaten, H., Lie, H., Tognarelli, M., 2005. Experimental investigation of vortex-induced vibration of long marine risers. Journal of Fluids and Structures 21 (3), 335–361.
Vandiver, J. K., Li, L., 2005. SHEAR7 V4.4 Program Theoretical Manual.
Vandiver, J. K., Swithenbank, S. B., Jaiswal, V., Jhingran, V., 2006. Fatigue damage from high mode number vortex-induced vibration. In: Proc. 25th OMAE Conf.
Venugopal, M., 1996. Damping and response prediction of a flexible cylinder in a current. Ph.D. thesis, Massachusetts Institute of Technology.
Vikestad, K., 1998. Multi-frequency response of a cylinder subjected to vortex shedding and support motions. Ph.D. thesis, Norwegian University of Science and Technology, Department of Marine Technology.
Vikestad, K., Larsen, C. M., Vandiver, J. K., et al., 2000. Norwegian deepwater program: damping of vortex-induced vibrations. In: Offshore Technology Conference. Offshore Technology Conference.
Williamson, C., Govardhan, R., 2004. Vortex-induced vibrations. Annual Review of Fluid Mechanics 36 (1), 413–455.
Wu, X., Ge, F., Hong, Y., 2012. A review of recent studies on vortex-induced vibrations of long slender cylinders. Journal of Fluids and Structures 28 (0), 292 – 308.
Yin, D., Larsen, C. M., 2012. Forced motion experiments with measured motions from flexible beam tests under uniform and sheared flows. In: ASME 2012 31st International Conference on Ocean, Offshore and Arctic Engineering. American Society of Mechanical Engineers, pp. 573–581.